



## Article

# Syntheses, Structures, and Properties of Mono- and Dinuclear Acetylacetonato Ruthenium(III) Complexes with Chlorido or Thiocyanato Ligands

Kai Nakashima <sup>1</sup>, Chihiro Hayami <sup>1</sup>, Shino Nakashima <sup>2</sup>, Haruo Akashi <sup>2</sup>, Masahiro Mikuriya <sup>3</sup> and Makoto Handa <sup>1,\*</sup>

<sup>1</sup> Department of Chemistry, Graduate School of Natural Science and Technology, Shimane University, 1060 Nishikawatsu, Matsue 690-8504, Japan; n22m620@matsu.shimane-u.ac.jp (K.N.); kendo1117.c.h@icloud.com (C.H.)

<sup>2</sup> Research Institute of Frontier Science and Technology, Okayama University of Science, 1-1 Ridaicho, Kita-Ku, Okayama 700-0005, Japan; s22cm10f@ous.jp (S.N.); akashi@ous.ac.jp (H.A.)

<sup>3</sup> School of Biological and Environmental Sciences, Kwansei Gakuin University, 1 Gakuen Uegahara, Sanda 669-1330, Japan; junpei@kwansei.ac.jp

\* Correspondence: handam@riko.shimane-u.ac.jp

**Abstract:** The mononuclear and dinuclear ruthenium(III) complexes *trans*-Ph<sub>4</sub>P[Ru<sup>III</sup>(acac)<sub>2</sub>Cl<sub>2</sub>] (**1**), Ph<sub>4</sub>P[*{Ru*<sup>III</sup>(acac)Cl]<sub>2</sub>(μ-Cl)<sub>3</sub>] (**2**) and *trans*-Ph<sub>4</sub>P[Ru<sup>III</sup>(acac)<sub>2</sub>(NCS)<sub>2</sub>]-0.5C<sub>6</sub>H<sub>14</sub> (**3**·0.5C<sub>6</sub>H<sub>14</sub>) were synthesized. Single crystals of **1**, **2**·H<sub>2</sub>O and **3**·CH<sub>3</sub>CN suitable for X-ray crystal structure analyses were obtained through recrystallization from DMF for **1** and **2**·H<sub>2</sub>O and from acetonitrile for **3**·CH<sub>3</sub>CN. An octahedral Ru with bis-chelate-acac ligands and axial chlorido or *κ*-N-thiocyanido ligands (for **1** and **3**·CH<sub>3</sub>CN) and triply μ-chlorido-bridged dinuclear Ru<sub>2</sub> for **2**·H<sub>2</sub>O were confirmed through the structure analyses. The Ru–Ru distance of 2.6661(2) of **2**·H<sub>2</sub>O is indicative of the existence of the direct metal–metal interaction. The room temperature magnetic moments ( $\mu_{\text{eff}}$ ) are 2.00 and 1.93  $\mu_{\text{B}}$  for **1** and **3**·0.5C<sub>6</sub>H<sub>14</sub>, respectively, and 0.66  $\mu_{\text{B}}$  for **2**. The temperature-dependent (2–300 K) magnetic susceptibility showed that the strong antiferromagnetic interaction ( $J \leq -800 \text{ cm}^{-1}$ ) is operative between the ruthenium(III) ions within the dinuclear core. In the <sup>1</sup>H NMR spectra measured in CDCl<sub>3</sub> at 298 K, the dinuclear complex **2** showed signals for the acac ligand protons at 2.50 and 2.39 ppm (for CH<sub>3</sub>) and 5.93 ppm (for CH), respectively, while **1** and **3**·0.5C<sub>6</sub>H<sub>14</sub> showed signals with large paramagnetic shifts; -17.59 ppm (for CH<sub>3</sub>) and -57.01 ppm (for CH) for **1** and -16.89 and -17.36 ppm (for CH<sub>3</sub>) and -53.67 and -55.53 ppm (for CH) for **3**·0.5C<sub>6</sub>H<sub>14</sub>. Cyclic voltammograms in CH<sub>2</sub>Cl<sub>2</sub> with an electrolyte of <sup>n</sup>Bu<sub>4</sub>N(ClO<sub>4</sub>) showed the Ru<sup>III</sup> → Ru<sup>IV</sup> redox wave at 0.23 V (vs. Fc/Fc<sup>+</sup>) for **1** and the Ru<sup>III</sup> → Ru<sup>II</sup> waves at -1.39 V for **1** and -1.25 V for **3**·0.5C<sub>6</sub>H<sub>14</sub> and the Ru<sup>III</sup>-Ru<sup>III</sup> → Ru<sup>III</sup>-Ru<sup>IV</sup> and Ru<sup>III</sup>-Ru<sup>III</sup> → Ru<sup>III</sup>-Ru<sup>IV</sup> waves at 0.91 V and -0.79 V for **2**.



**Citation:** Nakashima, K.; Hayami, C.; Nakashima, S.; Akashi, H.; Mikuriya, M.; Handa, M. Syntheses, Structures, and Properties of Mono- and Dinuclear Acetylacetonato Ruthenium(III) Complexes with Chlorido or Thiocyanato Ligands. *Magnetochemistry* **2024**, *10*, 16. <https://doi.org/10.3390/magnetochemistry10030016>

Academic Editor: Marius Andruh

Received: 26 January 2024

Revised: 21 February 2024

Accepted: 22 February 2024

Published: 27 February 2024



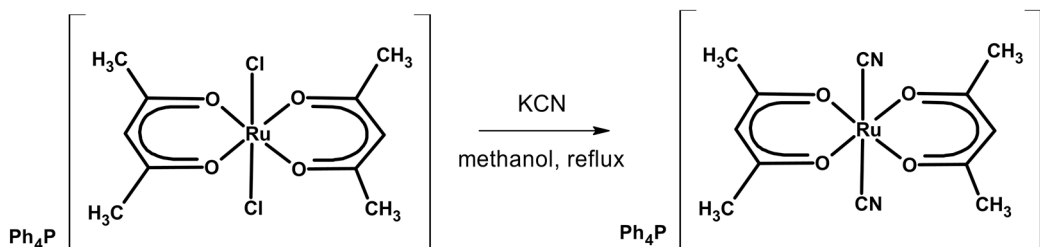
**Copyright:** © 2024 by the authors. Licensee MDPI, Basel, Switzerland. This article is an open access article distributed under the terms and conditions of the Creative Commons Attribution (CC BY) license (<https://creativecommons.org/licenses/by/4.0/>).

**Keywords:** mononuclear and dinuclear ruthenium (III) complex; acetylacetonato ligand; chlorido bridge; crystal structures; magnetic properties; antiferromagnetic interactions

## 1. Introduction

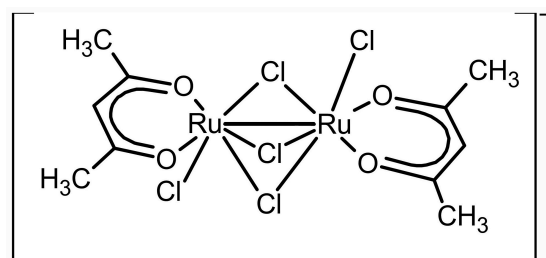
Acetylacetone (Hacac) is well known as one of useful bidentate ligands, which can form chelate complexes, such as [M<sup>II</sup>(acac)<sub>2</sub>], [M<sup>III</sup>(acac)<sub>3</sub>] and [M<sup>III</sup>(acac)<sub>2</sub>X<sub>2</sub>]<sup>-</sup>, through reactions with various transition metal ions [1–28]. The complexes have been widely investigated, for example, as building blocks for magnetic materials [29–31], NMR shift reagents and paramagnetic relaxation reagents [32–35] and catalysts [36,37]. The *trans*-[Ru<sup>III</sup>(acac)<sub>2</sub>(CN)<sub>2</sub>]<sup>-</sup> anion has an unpaired electron and has been reported to work as a paramagnetic linker in combination with Mn<sup>2+</sup> and [Fe<sup>III</sup>salen]<sup>+</sup> to produce ferri- or ferromagnetic compounds {Mn<sup>II</sup>[Ru<sup>III</sup>(acac)<sub>2</sub>(CN)<sub>2</sub>]<sub>2</sub>}<sub>n</sub> and {[Fe<sup>III</sup>(salen)]{Ru<sup>III</sup>(acac)<sub>2</sub>(CN)<sub>2</sub>}}<sup>-</sup> with two- and one-dimensional structures, respectively [38,39]. The cyanido linker anion

*trans*-[Ru<sup>III</sup>(acac)<sub>2</sub>(CN)<sub>2</sub>]<sup>−</sup> is prepared from *trans*-[Ru<sup>III</sup>(acac)<sub>2</sub>Cl<sub>2</sub>]<sup>−</sup> through the axial ligand substitution of Cl<sup>−</sup> with CN<sup>−</sup>, with the substitution reaction shown in Scheme 1 [38]. Through a research project, we studied using the anionic complex *trans*-[Ru<sup>III</sup>(acac)<sub>2</sub>(CN)<sub>2</sub>]<sup>−</sup> with more various metal ions or complexes to develop the chemistry of this type of assembled magnetic compounds.



**Scheme 1.** Axial ligand substitution reaction from *trans*-[Ru<sup>III</sup>(acac)<sub>2</sub>Cl<sub>2</sub>]<sup>−</sup> to *trans*-[Ru<sup>III</sup>(acac)<sub>2</sub>(CN)<sub>2</sub>]<sup>−</sup>.

During the course of our study, we found the formation of a dinuclear anion  $\{[\text{Ru}^{\text{III}}(\text{acac})\text{Cl}]_2(\mu\text{-Cl})_3\}^-$ , of which the structure is shown in Scheme 2, when the reaction of RuCl<sub>3</sub>·nH<sub>2</sub>O and Hacac was performed in the presence of KCl, followed by the addition of Ph<sub>4</sub>PCl to obtain *trans*-Ph<sub>4</sub>P[Ru<sup>III</sup>(acac)<sub>2</sub>Cl<sub>2</sub>] (**1**), and we could elucidate the dinuclear structure of Ph<sub>4</sub>P{[Ru<sup>III</sup>(acac)Cl]<sub>2</sub>(μ-Cl)<sub>3</sub>} (**2**) through an X-ray crystal structure analysis. Although Hasegawa et al. reported the formation of a dinuclear complex Ph<sub>4</sub>As{[Ru<sup>III</sup>(acac)Cl]<sub>2</sub>(μ-Cl)<sub>3</sub>} as a by-product when isolating *trans*-Ph<sub>4</sub>As[Ru<sup>III</sup>(acac)<sub>2</sub>Cl<sub>2</sub>], the dinuclear complex was characterized based on an elemental analysis and the <sup>1</sup>H NMR spectrum, their X-ray crystal structural data were incomplete to establish the dinuclear structure [40] and structurally elucidated examples of this kind of triply bridged diruthenium(III) complexes are still limited. Therefore, we decided to investigate the dinuclear complex Ph<sub>4</sub>P{[Ru<sup>III</sup>(acac)Cl]<sub>2</sub>(μ-Cl)<sub>3</sub>} (**2**) in more detail. For such a study, the mononuclear complexes *trans*-Ph<sub>4</sub>P[Ru<sup>III</sup>(acac)<sub>2</sub>Cl<sub>2</sub>] (**1**) and *trans*-Ph<sub>4</sub>P[Ru<sup>III</sup>(acac)<sub>2</sub>(NCS)<sub>2</sub>] (**3**) were also prepared and investigated. Here, we report on structures and magnetic, spectral, and electrochemical properties of *trans*-Ph<sub>4</sub>P[Ru<sup>III</sup>(acac)<sub>2</sub>Cl<sub>2</sub>] (**1**), Ph<sub>4</sub>P{[Ru<sup>III</sup>(acac)Cl]<sub>2</sub>(μ-Cl)<sub>3</sub>} (**2**) and *trans*-Ph<sub>4</sub>P[Ru<sup>III</sup>(acac)(NCS)<sub>2</sub>]·0.5C<sub>6</sub>H<sub>14</sub> (**3**·0.5C<sub>6</sub>H<sub>14</sub>).



**Scheme 2.** Chemical structure of  $\{[\text{Ru}(\text{acac})\text{Cl}]_2(\mu\text{-Cl})_3\}^-$ .

## 2. Results and Discussion

### 2.1. Synthesis and Characterizations

Refluxing a mixture of RuCl<sub>3</sub>·nH<sub>2</sub>O, acetylacetone (Hacac) and KCl in water and the addition of excess Ph<sub>4</sub>PCl gave the mononuclear complex *trans*-Ph<sub>4</sub>P[Ru<sup>III</sup>(acac)<sub>2</sub>Cl<sub>2</sub>] (**1**) in the yield of 11% (based on RuCl<sub>3</sub>). The chromatographical purifications with Al<sub>2</sub>O<sub>3</sub> columns (eluent: chloroform/MeOH and acetonitrile/chloroform) confirmed the formation of the dinuclear complex Ph<sub>4</sub>P{[Ru<sup>III</sup>(acac)Cl]<sub>2</sub>(μ-Cl)<sub>3</sub>} (**2**) in very low amounts. However, the yield of complex **2** increased to 1.6% (based on RuCl<sub>3</sub>) when passing oxygen gas through the reacting solution. The monomeric complex *trans*-Ph<sub>4</sub>P[Ru<sup>III</sup>(acac)<sub>2</sub>(NCS)<sub>2</sub>]·0.5C<sub>6</sub>H<sub>14</sub> (**3**·0.5C<sub>6</sub>H<sub>14</sub>) was synthesized by refluxing a methanolic solution of **1** and an excess amount

of KSCN in the yield of 64% (based on **1**). The chemical formulae of the obtained complexes of **1**, **2** and **3**·0.5C<sub>6</sub>H<sub>14</sub> were confirmed through elemental analyses. ESI-TOF-MS spectra also confirmed the formations of anionic units of 369.9307 *m/z* (calcd for [M]<sup>-</sup> 369.9318) for **1**, 577.7369 *m/z* (calcd for [M]<sup>-</sup> 577.6223) for **2** and 415.9426 *m/z* (calcd for [M]<sup>-</sup> 415.4562) for **3**·0.5C<sub>6</sub>H<sub>14</sub>. IR spectra of the complexes are given in Figures S1–S3. Powder X-ray diffraction (PXRD) analyses were also performed for complexes **1**, **2** and **3**·0.5C<sub>6</sub>H<sub>14</sub>. The obtained results are displayed in Figures S4–S6, respectively. The PXRD pattern of **1** agreed with its simulated pattern derived from the crystal structure of **1** (Figure S4). However, the patterns of **2** and **3**·0.5C<sub>6</sub>H<sub>14</sub> did not agree with those simulated from the crystal structures of **2**·H<sub>2</sub>O and **3**·CH<sub>3</sub>CN, respectively. The disagreement was more remarkable in **3**·0.5C<sub>6</sub>H<sub>14</sub>. The reason was explained to be the facts that crystals of **2**·H<sub>2</sub>O and **3**·CH<sub>3</sub>CN have the crystal solvents H<sub>2</sub>O and CH<sub>3</sub>CN, respectively, though the crystalline powder of **2** has no crystal solvent and that of **3**·0.5C<sub>6</sub>H<sub>14</sub> has solvent molecules of C<sub>6</sub>H<sub>14</sub>. Detailed discussions of the crystal structures of **1**, **2**·H<sub>2</sub>O and **3**·CH<sub>3</sub>CN are given in the next section.

## 2.2. Crystal Structures

Single crystals of **1** and **2**·H<sub>2</sub>O suitable for the X-ray crystal structure analysis were obtained through slow diffusion of diethyl ether to solutions of **1** and **2**·H<sub>2</sub>O in DMF, respectively, while, for **3**, the crystals were grown through recrystallization from acetonitrile and isolated as **3**·CH<sub>3</sub>CN. Crystallographic data are listed in Table 1. Selected bond distances and angles are given in Tables S1–S6, respectively. The mononuclear complex *trans*-Ph<sub>4</sub>P[Ru<sup>III</sup>(acac)<sub>2</sub>Cl<sub>2</sub>] (**1**) crystallized in the *P*<sub>1</sub> space group. The crystal packing diagram of **1** is shown Figure S7. In this crystal, there are crystallographically different mononuclear *trans*-[Ru<sup>III</sup>(acac)<sub>2</sub>Cl<sub>2</sub>]<sup>-</sup> anions designated as Ru1 and Ru2 for the central ruthenium atoms, while the tetraphenylphosphate (Ph<sub>4</sub>P<sup>+</sup>) cation exists among the [Ru<sup>III</sup>(acac)<sub>2</sub>Cl<sub>2</sub>]<sup>-</sup> units. The packing feature of the present complex is essentially the same as that for *trans*-Ph<sub>4</sub>As[Ru(acac)<sub>2</sub>Cl<sub>2</sub>] [40], though different counter cations of Ph<sub>4</sub>As<sup>+</sup> existed in the crystal. A perspective drawing of the structure of one of the [Ru<sup>III</sup>(acac)<sub>2</sub>Cl<sub>2</sub>]<sup>-</sup> units of **1** is shown in Figure 1. The inversion center is located at the ruthenium atom. The equatorial positions of each Ru atom are occupied with four oxygen atoms of the two acac ligands with Ru–O<sub>eq</sub> distances of 2.015(1) and 2.012(1) Å for Ru1 and 2.018(1) and 2.011(1) Å for Ru2, respectively, which are comparable to those of *trans*-Ph<sub>4</sub>As[Ru<sup>III</sup>(acac)<sub>2</sub>Cl<sub>2</sub>] (Ru–O<sub>eq</sub> = 2.010(3)–2.016(3) Å). The chlorido ligands are coordinated to Ru1 and Ru2 with distances of Ru–Cl<sub>ax</sub> = 2.360(1) and 2.363(1) Å, respectively, which are also comparable to those of *trans*-Ph<sub>4</sub>As[Ru<sup>III</sup>(acac)<sub>2</sub>Cl<sub>2</sub>] (Ru–Cl<sub>ax</sub> = 2.355(2) and 2.632(1) Å). The Cl<sub>ax</sub>–Ru–O<sub>eq</sub> bond angles are 88.46(4) and 91.54(4)° for Ru1 and 86.63(5) and 93.37(5)° for Ru2, respectively, of which values are comparable to those of *trans*-Ph<sub>4</sub>As[Ru(acac)<sub>2</sub>Cl<sub>2</sub>] ( $\angle$ Cl<sub>ax</sub>–Ru–O<sub>eq</sub> = 87.1(1)–91.5(1)°).

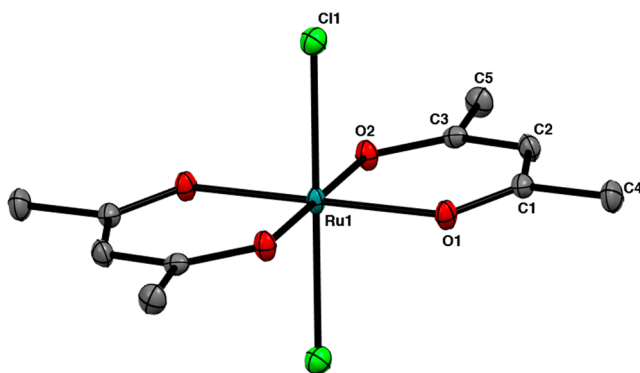


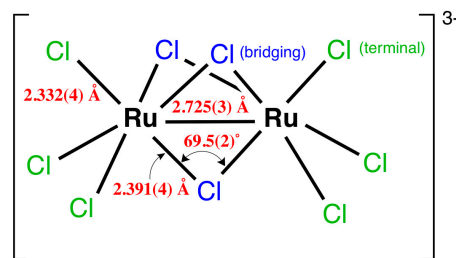
**Figure 1.** ORTEP view of one of the anionic units of **1**, showing thermal ellipsoids at the 50% probability level. Hydrogen atoms were omitted for clarity.

**Table 1.** Crystallographic data and structure refinement of **1**, **2**·H<sub>2</sub>O and **3**·CH<sub>3</sub>CN.

Complexes	<b>1</b>	<b>2</b> ·H <sub>2</sub> O	<b>3</b> ·CH <sub>3</sub> CN
Chemical formula	C <sub>34</sub> H <sub>34</sub> Cl <sub>2</sub> O <sub>4</sub> PRu	C <sub>34</sub> H <sub>36</sub> Cl <sub>5</sub> O <sub>5</sub> PRu <sub>2</sub>	C <sub>38</sub> H <sub>37</sub> N <sub>3</sub> O <sub>4</sub> PRuS <sub>2</sub>
FW	709.55	935.03	795.87
Temperature, T (K)	93	93	93
Crystal system	Triclinic	Triclinic	Monoclinic
Space group	P $\bar{1}$	P $\bar{1}$	P2 <sub>1</sub> /n
a (Å)	9.8418(2)	10.91020(10)	20.0627(3)
b (Å)	13.3562(3)	12.05510(10)	7.36340(10)
c (Å)	14.1498(2)	16.1720(2)	24.6645(5)
$\alpha$ (°)	103.441(2)	69.5690(10)	90
$\beta$ (°)	106.783(2)	74.3220(10)	98.403(2)
$\gamma$ (°)	107.998(2)	70.0890(10)	90
V (Å <sup>3</sup> )	1584.42(6)	1846.19(4)	3604.56(10)
Z	2	2	4
$D_{\text{calcd}}$ (g cm <sup>-3</sup> )	1.487	1.678	1.478
Crystal size (mm)	0.2 × 0.1 × 0.05	0.15 × 0.1 × 0.05	0.2 × 0.1 × 0.05
$\mu$ (mm <sup>-1</sup> )	0.751	1.263	0.643
$\theta$ range for data collection (°)	1.607–31.464	1.980–31.546	1.669–31.629
Reflections collected	30,580	34,229	67,229
[R <sub>1</sub> ( $I < 2\sigma(I)$ ); wR <sub>2</sub> (all data)] <sup>(a)</sup>	R <sub>1</sub> = 0.0301 wR <sub>2</sub> = 0.0826	R <sub>1</sub> = 0.0283 wR <sub>2</sub> = 0.0743	R <sub>1</sub> = 0.0310 wR <sub>2</sub> = 0.0947
GOF	1.106	1.072	1.099

$$(a) R_1 = \frac{\sum ||F_O|| - |F_C||}{\sum |F_O|}; \omega R_2 = \left[ \frac{\sum \omega (F_O^2 - F_C^2)^2}{\sum (F_O^2)^2} \right]^{\frac{1}{2}}.$$

The dinuclear complex Ph<sub>4</sub>P[{{Ru<sup>III</sup>(acac)Cl}<sub>2</sub>(μ-Cl)<sub>3</sub>}]<sup>3-</sup>·H<sub>2</sub>O (**2**·H<sub>2</sub>O) crystallized in P $\bar{1}$ . The crystal packing diagram and the dinuclear anionic unit of **2**·H<sub>2</sub>O are shown in Figure S8 and Figure 2, respectively. The crystal consists of Ph<sub>4</sub>P<sup>+</sup> cations, [{Ru<sup>III</sup>(acac)Cl}<sub>2</sub>(μ-Cl)<sub>3</sub>}<sup>3-</sup> anions and crystallization water molecules. There is no specific interaction between them. As shown in Figure S8, the dinuclear structure is composed of two Ru<sup>III</sup>(acac)Cl units with triple chlorido-bridges. Octahedral geometries around both the Ru(III) atoms are accomplished with the bidentate chelate of two acac ligands with Ru–O distances of 1.995(1) (for Ru1–O1), 1.991(1) (for Ru1–O2), 2.001(2) (for Ru2–O3) and 2.001(1) Å (for Ru2–O4), respectively. The chlorido bridges link the two ruthenium(III) atoms with distances of Ru1–Cl3 = 2.367(1), Ru1–Cl4 = 2.359(1), Ru1–Cl5 = 2.378(1), Ru2–Cl3 = 2.364(1), Ru2–Cl4 = 2.359(1) and Ru2–Cl5 = 2.378(1) Å. The bond distances are relatively long compared with those of the terminal Ru–Cl bonds in each Ru<sup>III</sup>(acac)Cl unit (Ru1–Cl1 = 2.340(1) and Ru2–Cl2 = 2.331(1) Å), reflecting the bridging property. The O–Ru–O chelate bite angles in the Ru<sup>III</sup>(acac)Cl units are close to 90° ( $\angle$ O1–Ru1–O2 = 93.60(6) and  $\angle$ O3–Ru2–O4 = 93.80(7)°). The face-sharing octahedral structure shown by **2**·H<sub>2</sub>O has been reported for the dinuclear complex Cs<sub>3</sub>[{Ru<sup>III</sup>Cl<sub>3</sub>}<sub>2</sub>(μ-Cl)<sub>3</sub>] [41]. The structure and bond distances and angles of the anionic unit, which has the D<sub>3h</sub> symmetry, are illustrated in Scheme 3.



**Scheme 3.** Chemical structure of [{Ru<sup>III</sup>Cl<sub>3</sub>}<sub>2</sub>(μ-Cl)<sub>3</sub>]<sup>3-</sup>, the bond distances and angles being shown together [41].

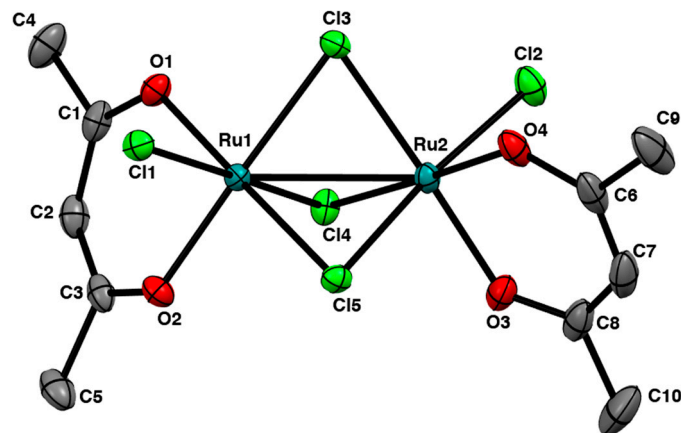
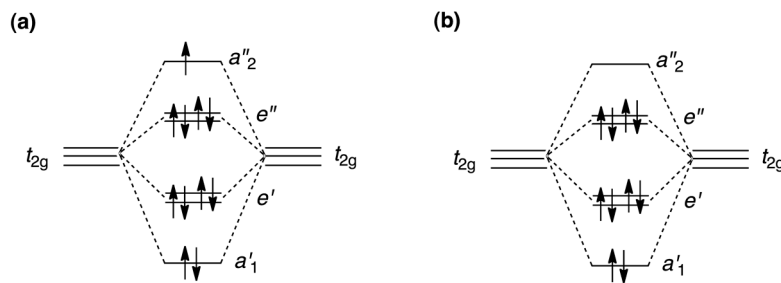


**Figure 2.** ORTEP view of the anionic dinuclear unit for  $\mathbf{2}\cdot\text{H}_2\text{O}$ , showing thermal ellipsoids at the 50% probability level. Hydrogen atoms were omitted for clarity.

The dimensions of the dinuclear cores of  $\text{Cs}_3[(\text{Ru}^{\text{III}}\text{Cl}_3)_2(\mu\text{-Cl})_3]$  and  $\mathbf{2}\cdot\text{H}_2\text{O}$  are very similar; Ru–Cl (terminal) = 2.332(4) Å (for  $\text{Cs}_3[(\text{Ru}^{\text{III}}\text{Cl}_3)_2(\mu\text{-Cl})_3]$ ) and 2.340(1) and 2.331(1) Å (for  $\mathbf{2}\cdot\text{H}_2\text{O}$ ), Ru–Cl (bridging) = 2.391(4) Å (for  $\text{Cs}_3[(\text{Ru}^{\text{III}}\text{Cl}_3)_2(\mu\text{-Cl})_3]$ ) and 2.359(1)–2.378(1) Å (for  $\mathbf{2}\cdot\text{H}_2\text{O}$ ), and  $\angle\text{Ru}-\text{Cl}(\text{bridging})-\text{Ru}$  = 69.5(2)° (for  $\text{Cs}_3[(\text{Ru}^{\text{III}}\text{Cl}_3)_2(\mu\text{-Cl})_3]$ ) and 68.36(1)–68.83(1)° (for  $\mathbf{2}\cdot\text{H}_2\text{O}$ ). The Ru–Ru distances are 2.725(3) Å for  $\text{Cs}_3[(\text{Ru}^{\text{III}}\text{Cl}_3)_2(\mu\text{-Cl})_3]$  and 2.6661(2) Å for  $\mathbf{2}\cdot\text{H}_2\text{O}$ , respectively. The short Ru–Ru distances are indicative of the direct M–M interaction between the ruthenium(III) ions. The mixed valent diruthenium(II,III) complexes with triply chlorido-bridges  $[(\text{Ru}^{2.5}(\text{NH}_3)_3)_2(\mu\text{-Cl})_3](\text{BPh}_4)_2$  and  $[(\text{Ru}^{2.5}(\text{tacn}))_2(\mu\text{-Cl})_3](\text{PF}_6)_2\cdot 4\text{H}_2\text{O}$  ( $\text{tacn}$  = 1,4,7-triazacyclononane) had similar, however, relatively longer, Ru–Ru distances, 2.753(4) Å for the former complex and 2.830(1) Å for the latter complex [42,43]. The mixed valence dinuclear complexes were interpreted to have an unpaired electron with an MO diagram for the eleven 4d electrons shown in Scheme 4a [43,44], where an unpaired electron resides in an  $a''_2$  ( $\sigma^*$ ) orbital and the bond order becomes 0.5. When this interpretation is applied to the  $\text{Ru}_{2}^{\text{III},\text{III}}$  complexes  $\mathbf{2}$  and  $\text{Cs}_3[(\text{Ru}^{\text{III}}\text{Cl}_3)_2(\mu\text{-Cl})_3]$ , the bond order becomes one, because an electron is removed from the  $a''_2$  ( $\sigma^*$ ) orbital, leading to relatively short Ru–Ru bonds. As discussed later, the diamagnetism of the  $\text{Ru}_{2}^{\text{III},\text{III}}$  complexes can be interpreted based on the MO diagram (Scheme 4b), where ten 4d electrons are arranged pairwise in the orbitals.



**Scheme 4.** MO diagram for 4d electrons of the mixed-valent diruthenium(II,III) (a) and diruthenium(III,III) (b) with the face-sharing octahedral structure [43,44].

The complex  $\mathbf{3}\cdot\text{CH}_3\text{CN}$  crystallized in the monoclinic lattice ( $P2_1/n$ ). The crystal consists of  $\text{Ph}_4\text{P}^+$  cations, *trans*- $[\text{Ru}^{\text{III}}(\text{acac})_2(\text{NCS})_2]^-$  anions and crystallization solvent molecules of  $\text{CH}_3\text{CN}$ , as can be seen in the packing diagram (Figure S9). The anionic unit of *trans*- $[\text{Ru}^{\text{III}}(\text{acac})_2(\text{NCS})_2]^-$  is shown in Figure 3. The Ru–O<sub>eq</sub> (acac) distances are 2.002(1)–2.012(1) Å, comparable to those of  $\mathbf{1}$  and  $\mathbf{2}\cdot\text{H}_2\text{O}$ . The Ru(III) center is further coordinated by nitrogen atoms of the NCS<sup>−</sup> ligands with Ru–N bond distances of 2.016(2) (for Ru1–N1) and 2.007(2) Å (for Ru1–N2), respectively. The bond angles of O1–Ru1–O2,

O1–Ru1–O3, O2–Ru–O4 and O3–Ru1–O4 are 93.71(5), 85.99(5), 87.03(5) and 93.28(5) $^{\circ}$ , respectively. The sum of the four  $\angle$ O<sub>eq</sub>–Ru–O<sub>eq'</sub> values is 360.0 $^{\circ}$ , which indicates that the ruthenium atom is located without deviation on the plane composed of oxygen atoms O1, O2, O3 and O4. Although three atoms of each NCS<sup>−</sup> ligands are arranged almost linearly ( $\angle$ N1–C11–S1 = 178.9(2) and  $\angle$ N2–C12–S2 = 177.9(2) $^{\circ}$ ), the bond angle values of  $\angle$ Ru1–N1–C11 = 170.9(1) and  $\angle$ Ru1–N2–C12 = 173.0(1) means that the axial coordination of the NCS<sup>−</sup> ligands are slightly tilted from the perpendicular vector to the Ru(O<sub>eq</sub>)<sub>4</sub> plane, while the N1–Ru1–N2 bond angle (177.5(1) $^{\circ}$ ) is close to 180 $^{\circ}$ .

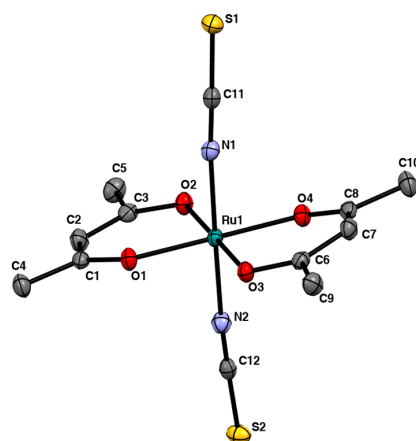


**Figure 3.** ORTEP view of the anionic unit for **3**·CH<sub>3</sub>CN, showing thermal ellipsoids at the 50% probability level. Hydrogen atoms were omitted for clarity.

As can be seen from the bond distances and angles for the cations of Ph<sub>4</sub>P<sup>+</sup> listed in Tables S1–S6, the structural features of the cations are basically the same among the complexes **1**, **2**·H<sub>2</sub>O and **3**·CH<sub>3</sub>CN.

### 2.3. Magnetic Properties

The temperature dependencies of the effective magnetic moment ( $\mu_{\text{eff}}$ ) (per Ru(III)) for **1** and **3**·0.5C<sub>6</sub>H<sub>14</sub> and per Ru(III)<sub>2</sub> for **2**) and reciprocal magnetic susceptibility (1/ $\chi_M$ ) values of **1**, **2** and **3**·0.5C<sub>6</sub>H<sub>14</sub> are given in Figures 4–6, respectively. The temperature-dependent behaviors are essentially different between the mononuclear complexes **1** and **3**·0.5C<sub>6</sub>H<sub>14</sub> and the dinuclear complex **2**.

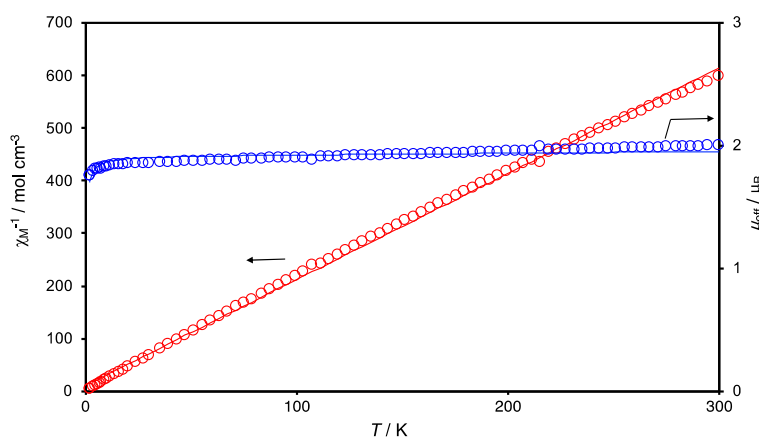


**Figure 4.** Temperature dependences of reciprocal magnetic susceptibility 1/ $\chi_M$  (red circles) and magnetic moment  $\mu_{\text{eff}}$  (blue circles) of *trans*-Ph<sub>4</sub>P[Ru<sup>III</sup>(acac)<sub>2</sub>Cl<sub>2</sub>] (**1**). The red solid line was drawn with  $C = 0.498 \text{ cm}^3 \text{ mol}^{-1} \text{ K}$  and  $\theta = -6.3 \text{ K}$  and the blue solid line was calculated and drawn with  $g = 2.21$ ,  $J = -0.29 \text{ cm}^{-1}$  and  $N\alpha = 60 \times 10^{-6} \text{ emu mol}^{-1}$  (see text).

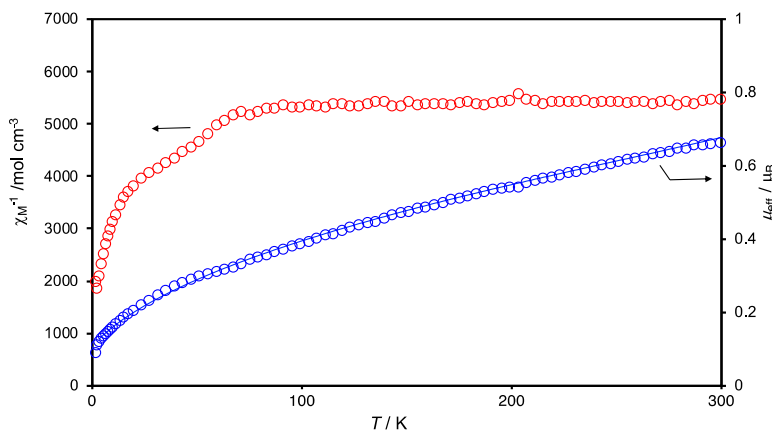


**Figure 5.** Temperature dependencies of reciprocal magnetic susceptibility  $\chi_M$  (red circles) and magnetic moment  $\mu_{\text{eff}}$  (blue circles) for  $\text{Ph}_4\text{P}[\{\text{Ru}^{\text{III}}(\text{acac})\text{Cl}\}_2(\mu\text{-Cl})_3]$  (**2**). The blue solid line was calculated and drawn with the parameter values of  $g = 2.2$ ,  $J = -800 \text{ cm}^{-1}$ ,  $N\alpha = 90 \times 10^{-6} \text{ emu mol}^{-1}$  and  $\rho = 0.0015$  (see text).

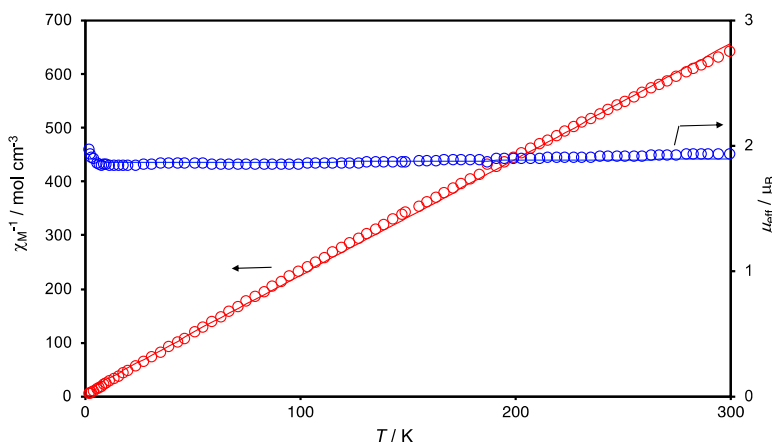


**Figure 6.** Temperature dependences of reciprocal magnetic susceptibility  $1/\chi_M$  (red circles) and magnetic moment  $\mu_{\text{eff}}$  of *trans*- $\text{Ph}_4\text{P}[\text{Ru}^{\text{III}}(\text{acac})_2(\text{NCS})_2]$  (**3**· $0.5\text{C}_6\text{H}_{14}$ ). The red solid line was drawn with  $C = 0.464 \text{ cm}^3 \text{ mol}^{-1} \text{ K}$  and  $\theta = -4.8 \text{ K}$  and the blue solid line was calculated and drawn with  $g = 2.14$ ,  $J = 0.22 \text{ cm}^{-1}$  and  $N\alpha = 60 \times 10^{-6} \text{ emu mol}^{-1}$  (see text).

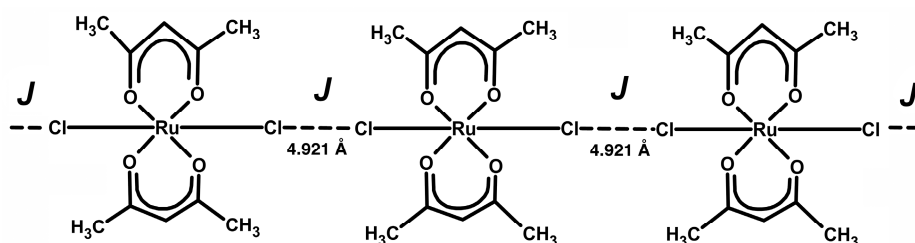
The magnetic moments at 300 K are 2.00 and  $1.93 \mu_B$  for **1** and **3**· $0.5\text{C}_6\text{H}_{14}$ , respectively, indicating the existences of an unpaired electron for both the complexes when considering that the spin-only value is  $1.73 \mu_B$  for an  $S = 1/2$  system. Although both of the complexes have rather large moment values, the temperature dependences of  $\chi_M^{-1}$  obey the Curie–Weiss law,  $\chi_M = C/(T - \theta)$  with  $C = 0.498 \text{ cm}^3 \text{ mol}^{-1} \text{ K}$  and  $\theta = -6.3 \text{ K}$  for **1** and  $C = 0.464 \text{ cm}^3 \text{ mol}^{-1} \text{ K}$  and  $\theta = -4.8 \text{ K}$  for **3**· $0.5\text{C}_6\text{H}_{14}$ , meaning that the interaction between the mononuclear Ru(III) units is limited and weakly antiferromagnetic overall. A difference in the temperature-dependent profile between **1** and **3**· $0.5\text{C}_6\text{H}_{14}$  was observed when the temperature fell below 5 K; the moment value ( $\mu_{\text{eff}}$ ) decreased for **1** and increased for **3**· $0.5\text{C}_6\text{H}_{14}$ , which may have occurred due to the difference in the weak interaction between **1** and **3**· $0.5\text{C}_6\text{H}_{14}$ . We looked into the X-ray crystal structure data of **1** and **3**· $\text{CH}_3\text{CN}$  to search the origin of such interactions. The closest distance between chlorine atoms (designated with Cl1 and Cl2) of neighboring  $[\text{Ru}(\text{acac})_2\text{Cl}_2]^-$  units is 4.921 Å for **1** (see Figure S7), leading to a chain structure, as shown in Scheme 5, and that between sulfur atoms (designated with S2) of  $[\text{Ru}(\text{acac})_2(\text{NCS})_2]^-$  units is 4.980 Å (the second and third closest distances are considerably long; 7.363 and 7.539 Å for S1···S1 separation) (see Figure S9), leading to a dimer structure, as shown in Scheme 6. Taking these contacts (4.921 Å for **1** and 4.980 Å for **3**· $\text{CH}_3\text{CN}$ ) into consideration, we analyzed their temperature-

dependent magnetic moments with the equation introduced by Bonner–Fisher for the chain  $S = 1/2$  local spins (Equation (1)) in the case of **1** (see Scheme 5) [45] and the Bleaney–Bowers equation for the two  $S = 1/2$  local spins (Equation (2)) in the case of **3** (see Scheme 6) [46].

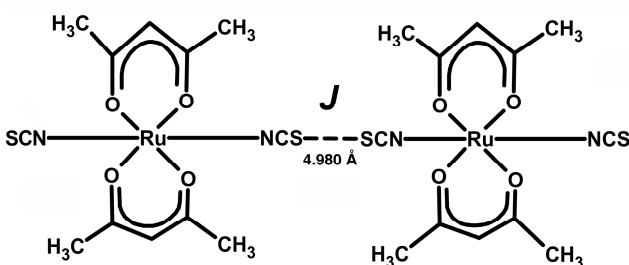
$$\chi_M = (Ng^2\beta^2/kT)(0.25 + 0.14995x + 0.30094x^2)/(1.0 + 1.9862x + 0.68854x^2 + 6.062x^3) + N\alpha, \text{ with } x = |J|/kT \quad (1)$$

$$\chi_M = 2(Ng^2\beta^2/kT)[3 + \exp(-2J//kT)]^{-1} + 2N\alpha \quad (2)$$

where  $N$  is the Avogadro number,  $g$  is the  $g$  factor,  $\beta$  is the Bohr magneton,  $k$  is the Boltzmann constant,  $J$  is the exchange integral between the ruthenium (III) ions and  $N\alpha$  is the temperature-independent paramagnetism (TIP). The temperature-dependent profiles could be reproduced with the parameter values of  $g = 2.21$ ,  $J = -0.29 \text{ cm}^{-1}$  and  $N\alpha = 60 \times 10^{-6} \text{ emu mol}^{-1}$  for **1** and  $g = 2.14$ ,  $J = 0.22 \text{ cm}^{-1}$  and  $N\alpha = 60 \times 10^{-6} \text{ emu mol}^{-1}$  for **3**·0.5C<sub>6</sub>H<sub>14</sub>, which are included as blue solid lines in Figures 4 and 6, respectively. The results support that the Cl···Cl (=4.921 Å in **1**) and S···S (=4.980 Å in **3**·CH<sub>3</sub>CN) contacts found in the crystal structures gave rise to the weak antiferromagnetic and ferromagnetic interactions observed below 5 K in **1** and **3**·0.5C<sub>6</sub>H<sub>14</sub>, respectively.



**Scheme 5.** Chain structure comprised of  $[\text{Ru}(\text{acac})_2\text{Cl}_2]^-$  units in **1**.  $J$  is the parameter for the magnetic interaction between  $[\text{Ru}(\text{acac})_2\text{Cl}_2]^-$  units in the chain.



**Scheme 6.** Dimer structure comprised of  $[\text{Ru}(\text{acac})_2(\text{NCS})_2]^-$  units in **3**.  $J$  is the parameter for the magnetic interaction between  $[\text{Ru}(\text{acac})_2(\text{NCS})_2]^-$  units in the dimer.

The magnetic moment ( $\mu_{\text{eff}}$ ) of **2** is  $0.66 \mu_B$  at 300 K, which is much lower than the spin-only value ( $1.73 \mu_B$ ), indicating the existence of a strong antiferromagnetic interaction in the anionic unit of  $[\{\text{Ru}^{\text{III}}(\text{acac})_2(\mu\text{-Cl})_3\}]^-$ . In fact, due to the strong antiferromagnetic interaction, the temperature dependence of  $\chi_M^{-1}$  no longer obeys the Curie–Weiss law (Figure 5). The magnetic moment decreases steadily with lowering the temperature. Due to each Ru(III) center having an unpaired electron ( $S = 1/2$ ), the magnetic behavior was simulated using the modified Bleaney–Bowers equation (Equation (3)), including a correction term ( $\rho$ ) for paramagnetic impurities:

$$\chi_M = 2\{(1 - \rho)(Ng^2\beta^2/kT)[3 + \exp(-2J//kT)]^{-1} + \rho(Ng^2\beta^2/4kT) + N\alpha\} \quad (3)$$

The simulation results gave the following parameter values:  $g = 2.2$ ,  $J \leq -800 \text{ cm}^{-1}$ ,  $N\alpha = 90 \times 10^{-6} \text{ emu mol}^{-1}$ ,  $\rho = 0.0015$ . The fitting quality was nearly the same, as long as  $J \leq -800 \text{ cm}^{-1}$ , when other parameter values were fixed at  $g = 2.2$ ,  $N\alpha = 90 \times 10^{-6} \text{ emu mol}^{-1}$ , and  $\rho = 0.0015$ . This large negative  $J$  value ( $J \leq -800 \text{ cm}^{-1}$ ) obviously means that there is a very strong antiferromagnetic interaction between the Ru(III) centers, leading to

the fact that complex **2** is practically diamagnetic ( $\mu_{\text{eff}} = 0.66 \mu_B$ ). The dinuclear complex  $\text{Cs}_3[(\text{Ru}^{\text{III}}\text{Cl}_3)_2(\mu\text{-Cl})_3]$  was reported to have a moment value of  $\mu_{\text{eff}} = 0.51 \mu_B$  at 300 K [41], indicating that the strong antiferromagnetic interaction is also operative between the Ru(III) centers, like in the case of **2**. As to this type of face-sharing bioctahedral complex anion  $[(\text{Ru}^{\text{III}}\text{Cl}_3)_2(\mu\text{-Cl})_3]^{3-}$ , calculations using the broken-symmetry density functional theory have been performed [47]. The calculation results indicated that the Ru(III) ions (low-spin state) were strongly coupled to result in the formation of a metal–metal  $\sigma$  bond and the minimum energy was at  $\text{Ru–Ru} = 2.74 \text{ \AA}$ , which was in good agreement with the observed bond length value of  $\text{Ru–Ru} = 2.725(3) \text{ \AA}$  for  $\text{Cs}_3[(\text{Ru}^{\text{III}}\text{Cl}_3)_2(\mu\text{-Cl})_3]$ . Due to  $2\text{-H}_2\text{O}$  having nearly the same Ru–Ru distance ( $2.6661(2) \text{ \AA}$ ) as that of  $\text{Cs}_3[(\text{Ru}^{\text{III}}\text{Cl}_3)_2(\mu\text{-Cl})_3]$ , the strong antiferromagnetic interaction ( $J \leq -800 \text{ cm}^{-1}$ ) is considered to be based on the direct interaction between the Ru(III) centers and pairwise arrangement of ten 4d electrons in the molecular orbitals (Scheme 4b).

The Ru–Ru distance is an important piece of evidence used to determine the presence of the direct metal–metal interactions. But this is not enough, like in the case of the face-sharing octahedral complex  $\{[\text{Ru}^{\text{III}}\text{Cl}_2(^n\text{Bu}_3\text{P})]\{\text{Ru}^{\text{III}}\text{Cl}(^n\text{Bu}_3\text{P})\}(\mu\text{-Cl})_3\}$ , which had a rather long Ru–Ru distance of  $3.176(1) \text{ \AA}$ , and it was difficult to determine whether or not the direct interaction existed. The magnetic susceptibility data could have given the answer to the question, although this complex was obtained only once, in a very small amount, as single crystals and no magnetic measurement has been carried out [48].

Field-dependent magnetizations were measured at 2K for **1**, **2** and **3**·0.5C<sub>6</sub>H<sub>14</sub>, the results being given in Figures S10, S11 and S12, respectively. On the increase in the external magnetic field, magnetizations of **1** and **3**·0.5C<sub>6</sub>H<sub>14</sub> increased to 1.10 and 0.94 N $\beta$ , respectively, at 70,000 Oe. Brillouin function curves with  $g = 2.3$  for **1** and  $g = 2.1$  for **3**·0.5C<sub>6</sub>H<sub>14</sub> were drawn with red solid lines in Figures S10 and S12, respectively. The deviation from the theoretical curve (Brillouin function) could have occurred due to the magnetic anisotropy and/or magnetic interactions. The field dependence for the magnetization of **2** is typical of the one for diamagnetism due to the strong antiferromagnetic interaction between the two Ru(III) ions (Figure S11).

#### 2.4. Reflectance and Absorption Spectra

Diffuse reflectance and absorption spectra for **1**, **2** and **3**·0.5C<sub>6</sub>H<sub>14</sub> were measured in solid and solution (CH<sub>2</sub>Cl<sub>2</sub>) and given in Figure S13 and Figure 7, respectively. As to *trans*-Ph<sub>4</sub>As[Ru<sup>III</sup>(acac)<sub>2</sub>Cl<sub>2</sub>], which have been measured in MeOH, Hasegawa et al. assigned the lowest energy band at 521 nm as  $\pi d \leftarrow \pi$  (acac<sup>-</sup>) and the second lowest energy band at 376 nm as  $\pi d \leftarrow \text{Cl}^-$ , referring to the assignment reported for [Ru<sup>III</sup>(acac)<sub>3</sub>] [40,49]. The assignment is also applicable for complexes **1**, **2** and **3**·0.5C<sub>6</sub>H<sub>14</sub>. The similarity in the band positions between the reflectance and absorption spectra indicates that the mononuclear and dinuclear core structures (*trans*-[Ru<sup>III</sup>(acac)<sub>2</sub>Cl<sub>2</sub>]<sup>-</sup> (for **1**),  $\{[\text{Ru}^{\text{III}}(\text{acac})\text{Cl}]_2(\mu\text{-Cl})_3\}^-$  (for **2**) and *trans*-[Ru<sup>III</sup>(acac)<sub>2</sub>(NCS)<sub>2</sub>]<sup>-</sup> (for **3**·0.5C<sub>6</sub>H<sub>14</sub>) are maintained in the solution.

#### 2.5. <sup>1</sup>H NMR Spectra

The <sup>1</sup>H NMR spectra were measured for **1**, **2** and **3**·0.5C<sub>6</sub>H<sub>14</sub> in chloroform-d<sub>1</sub> at 298 K, and are given in Figures S14, S15 and S16, respectively. In the case of **2**, other than the signals at 7.8–8.1 ppm for the phenyl protons of Ph<sub>4</sub>P<sup>+</sup>, signals at 2.39 and 2.50 ppm and at 5.93 ppm were observed; the set of the former two signals and the latter signal was assigned as methyl (CH<sub>3</sub>) and methine (CH) protons, respectively, for the acac ligand. It should be noted that the signals appeared in this region due to the strong antiferromagnetic interaction within the dinuclear anion of **2** to be diamagnetic. Although the reason for the splitting of the signals for the methyl protons (CH<sub>3</sub>) is unclear, a similar assignment had been determined for the signals for the protons of the dinuclear complex *trans*-Ph<sub>4</sub>As[Ru<sup>III</sup>(acac)<sub>2</sub>Cl<sub>2</sub>] measured in acetone-d<sub>6</sub> (2.40 (6H, s, CH<sub>3</sub>), 2.46 (6H, s, CH<sub>3</sub>), 5.99 (~2H, s, CH), 7.90 (16H, m, o, m-H) and 7.96 ppm (4H, t, p-H)) [40]. In the cases of the mononuclear complexes **1** and **3**·0.5C<sub>6</sub>H<sub>14</sub>, large paramagnetic shifts were observed

for the signals of the acac ligand protons ( $-17.59$  ppm (for  $\text{CH}_3$ ) and  $-57.01$  ppm (for  $\text{CH}$ ) for **1** and  $-16.89$  and  $-17.36$  ppm (for  $\text{CH}_3$ ) and  $-53.67$  and  $-55.53$  ppm (for  $\text{CH}$ ) for **3** $\cdot$ 0.5C<sub>6</sub>H<sub>14</sub> other than the phenyl protons of Ph<sub>4</sub>P<sup>+</sup>; the signals for the  $\text{CH}_3$  and  $\text{CH}$  protons of **3** $\cdot$ 0.5C<sub>6</sub>H<sub>14</sub> are split, respectively.

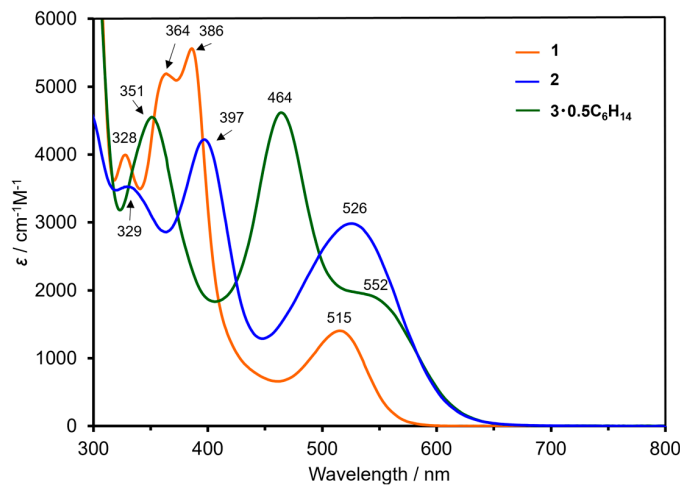


**Figure 7.** Absorption spectra (measured in CH<sub>2</sub>Cl<sub>2</sub>) of **1** (orange line), **2** (blue line) and **3** $\cdot$ 0.5C<sub>6</sub>H<sub>14</sub> (green line).

## 2.6. Cyclic Voltammograms

Cyclic voltammograms (CVs) were obtained for **1**, **2** and **3** $\cdot$ 0.5C<sub>6</sub>H<sub>14</sub> in dichloromethane solutions containing 0.1 M of  ${}^n\text{Bu}_4\text{N}(\text{ClO}_4)$ . The voltammograms of **1** and **2** are given in Figure 8. Complex **1** showed a redox wave at  $E_{1/2} ((E_{\text{pa}} + E_{\text{pc}})/2) = 0.23$  V (vs. Fc/Fc<sup>+</sup>), which was attributed to the Ru<sup>III</sup>  $\rightarrow$  Ru<sup>IV</sup> process, and an irreversible wave at  $E_{1/2} (E_{\text{pc}}/2) = -1.39$  V, which was attributed to the Ru<sup>III</sup>  $\rightarrow$  Ru<sup>II</sup> process. Hasegawa et al. reported that the corresponding waves were observed at 0.93 and  $-0.45$  V (vs. NHE) for *trans*-Ph<sub>4</sub>As[Ru<sup>III</sup>(acac)<sub>2</sub>Cl<sub>2</sub>] in the acetone solution, the potential values being calculated to be 0.29 and  $-1.09$  V (vs. Fc/Fc<sup>+</sup>), respectively [40], when quoting  $E_{1/2} = 0.64$  V (vs. NHE) for the Fc/Fc<sup>+</sup> redox couple in the literature [50]. The dinuclear complex **2** showed a redox wave at  $E_{1/2} = 0.91$  V and another wave at  $E_{1/2} = -0.79$  V. The former wave was attributed to the Ru<sup>III</sup> $\text{--}$ Ru<sup>III</sup>  $\rightarrow$  Ru<sup>III</sup> $\text{--}$ Ru<sup>IV</sup> process, and the latter wave was attributed to the Ru<sup>III</sup> $\text{--}$ Ru<sup>III</sup>  $\rightarrow$  Ru<sup>II</sup> $\text{--}$ Ru<sup>III</sup> process.

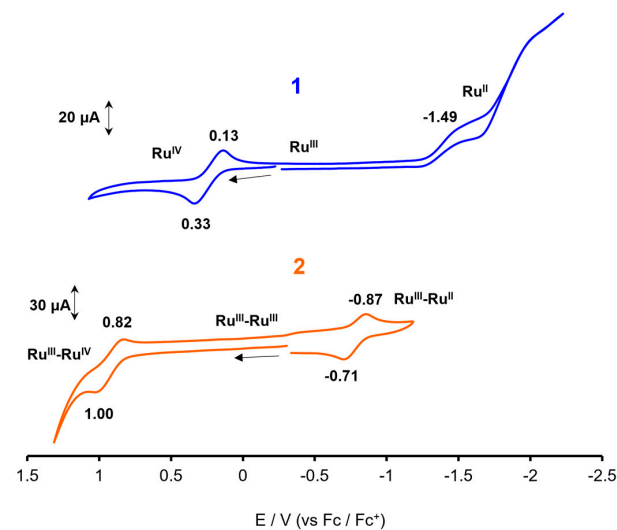


**Figure 8.** Cyclic voltammograms of **1** (blue line) and **2** (orange line) at  $1.0 \times 10^{-3}$  M in CH<sub>2</sub>Cl<sub>2</sub> containing 0.1 M  ${}^n\text{Bu}_4\text{N}(\text{ClO}_4)$  (glassy carbon working electrode; scan rate = 50 mV/s; room temperature; under Ar).

Complex **3**·0.5C<sub>6</sub>H<sub>14</sub> showed a rather complicated redox behavior. As shown in Figure 9, in the oxidation process, irreversible waves were observed. They should have been related to the oxidation of the NCS<sup>-</sup> ligands and decomposition of the complex [51] because a quasi-reversible redox wave at  $E_{1/2} = -1.25$  V disappeared when the CV measurement started toward the oxidation side. The redox wave at  $-1.25$  V was attributed to the Ru<sup>III</sup> → Ru<sup>II</sup> process and positively shifted compared with that for **1** ( $-1.39$  V), probably due to the stronger donating nature of NCS<sup>-</sup> (in **3**·0.5C<sub>6</sub>H<sub>14</sub>) than Cl<sup>-</sup> (in **1**).

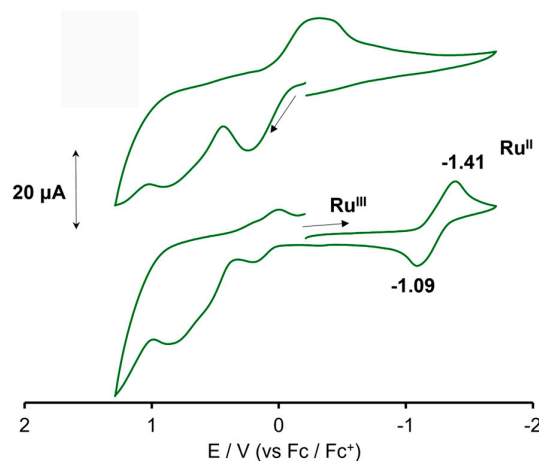


**Figure 9.** Cyclic voltammograms of **3**·0.5C<sub>6</sub>H<sub>14</sub> at  $1.0 \times 10^{-3}$  M in CH<sub>2</sub>Cl<sub>2</sub> containing 0.1 M <sup>n</sup>Bu<sub>4</sub>N(ClO<sub>4</sub>) (glassy carbon working electrode; scan rate = 50 mV/s; room temperature; under Ar).

### 3. Materials and Methods

#### 3.1. General Aspects

The elemental analyses for C, H and N were carried out using YANACO CHN CORDER MT-6 (Yanako, Tokyo, Japan). Infrared spectra were recorded as KBr disk using a JASCO FT/IR-4600 (JASCO, Tokyo, Japan). Powder X-ray diffraction analysis was performed on a Rigaku SmartLab X-ray diffractometer (Rigaku, Tokyo, Japan) with Cu K $\alpha$ . Magnetic susceptibilities were measured by using Quantum Design MPMS-XL7 (Quantum Design, San Diego, CA, USA) (installed at the Institute of Molecular Science (IMS), Okazaki, Japan) for **1** and **3**·0.5C<sub>6</sub>H<sub>14</sub> and MPMS3 (Quantum Design, San Diego, CA, USA) (installed at Shimane University) for **2** over the temperature range of 2–300 K with a magnetic field of 5000 Oe. The measured data were corrected for diamagnetic contribution [52]. Field-dependent magnetization measurements were performed from 0 to 70,000 Oe at 2 K for **1**, **2** and **3**·0.5C<sub>6</sub>H<sub>14</sub> with MPMS 3. Absorption and diffuse reflectance spectra were measured with Shimadzu UV-2450 (Shimadzu, Kyoto, Japan). Cyclic voltammograms were obtained in dichloromethane containing 0.1 M of tetra-*n*-butylammonium perchlorate (<sup>n</sup>Bu<sub>4</sub>N(ClO<sub>4</sub>)) on a BAS 100BW Electrochemical Workstation (Bioanalytical Systems, West Lafayette, IN, USA). A glassy carbon disk (1.5 mm radius), a platinum wire and a Ag/Ag<sup>+</sup> (TBAP/CH<sub>3</sub>CN) electrode were used as the working, counter and reference electrodes, respectively. Ferrocene (Fc) was used as an internal standard, and the potentials were quite relative to the Fc/Fc<sup>+</sup> couple. ESI-TOF-MS spectra were recorded on a Bruker micrOTOF II (Bruker, Billerica, MA, USA) with an acetonitrile solution. <sup>1</sup>H spectra were obtained with a JEOL JNM-AL 400 spectrometer (JEOL, Tokyo, Japan) in chloroform-*d*<sub>1</sub>. Chemical shifts ( $\delta$ /ppm) were determined using the residual solvent signal: 7.26 ppm for the proton of CHCl<sub>3</sub> in CDCl<sub>3</sub> for <sup>1</sup>H NMR spectra [53,54].

#### 3.2. Synthesis of Complexes

##### 3.2.1. Synthesis of trans-Ph<sub>4</sub>P[Ru<sup>III</sup>(acac)<sub>2</sub>Cl<sub>2</sub>] (**1**)

This complex was synthesized using a modified method described in the literature [40]. A mixture of RuCl<sub>3</sub>·*n*H<sub>2</sub>O (0.40 g, 1.93 mmol (based on RuCl<sub>3</sub>)), acetylacetone (2 mL) and

1 M KCl in water (2 mL) was refluxed for 30 min. Then, the solution was evaporated to dryness and the residue was dissolved in *c.a.* 20 mL of water. The addition of Ph<sub>4</sub>PCl (0.36 g, 0.961 mmol) in 2 mL of water to the solution gave an orange precipitate, which was collected and dried over P<sub>2</sub>O<sub>5</sub> under vacuum overnight. The obtained orange powder was dissolved in chloroform and purified chromatographically using an Al<sub>2</sub>O<sub>3</sub> column (eluent: chloroform/methanol (99:1 *v/v*.). The second fraction separated from the small amount of the first fraction was evaporated to dryness and employed again for chromatographic purification using an Al<sub>2</sub>O<sub>3</sub> column (eluent: methanol/acetonitrile (1:1 *v/v*.). The eluent was evaporated to dryness, dissolved in a small amount of chloroform, followed by the addition of *n*-hexane, giving an orange precipitation, which was collected through filtration and dried under vacuum at 100 °C for 3 h. The yield was 0.15g (11%, based on RuCl<sub>3</sub>). Anal. found: C; 56.94, H; 4.73. calcd for C<sub>34</sub>H<sub>34</sub>Cl<sub>2</sub>O<sub>4</sub>PRu: C; 57.55, H; 4.83. IR data (KBr disk, cm<sup>-1</sup>) 3059 w, 1585 w, 1546 s, 1520 vs, 1482 w, 1435 m, 1387 s, 1267 m, 1199 w, 1164 w, 1109 s, 1022 w, 997 w, 935 w, 788 w, 755 w, 726 s, 693 s, 660 m, 526 s, 456 m. UV–Vis (in CH<sub>2</sub>Cl<sub>2</sub>,  $\lambda_{\text{max}}$ ) 515, 386, 364, 328, 276, 232 nm. HR-MS (ESI-TOF) 369.9307 *m/z* (calcd for [M]<sup>+</sup> 369.9318). <sup>1</sup>H NMR (chloroform-*d*<sub>1</sub>, 298 K)  $\delta$  9.00–8.00 (m, *o, m, p*-H), –17.59 (s, CH<sub>3</sub>), –57.01 (br.s., CH).

### 3.2.2. Synthesis of Ph<sub>4</sub>P[{{Ru<sup>III</sup>(acac)Cl}<sub>2</sub>(μ-Cl)<sub>3</sub>}] (2)

A mixture of RuCl<sub>3</sub>·*n*H<sub>2</sub>O (0.31 g, 1.49 mmol (based on RuCl<sub>3</sub>)), acetylacetone (1.5 mL) and 1.0 M aqueous solution of KCl (1.5 mL) was refluxed for 30 min. During the reaction, oxygen gas was passed through the reacting solution. Then, the solution was evaporated to dryness and the residue was dissolved in *c.a.* 30 mL of water. Ph<sub>4</sub>PCl (0.30 g, 0.81 mmol) was added to the aqueous solution, giving a purple precipitate, which was collected through suction filtration. The obtained powder was dissolved in chloroform and purified chromatographically using an Al<sub>2</sub>O<sub>3</sub> column (eluent: chloroform/methanol (10:3 *v/v*.)). The first fraction was evaporated to dryness and employed again for chromatographic purification using an Al<sub>2</sub>O<sub>3</sub> column (eluent: chloroform/acetonitrile (1:1 *v/v*.)). The eluted solution was evaporated to dryness and dissolved in a small amount of chloroform, followed by the addition of *n*-hexane to give a purple precipitate, which was collected through filtration and dried under vacuum at 110 °C for 3 h. The yield was 0.021 g (1.6% based on RuCl<sub>3</sub>). Anal found: C, 44.27, H, 3.64. calcd for C<sub>34</sub>H<sub>34</sub>Cl<sub>5</sub>O<sub>4</sub>PRu<sub>2</sub>: C, 44.53, H, 3.74. IR data (KBr disk, cm<sup>-1</sup>) 3056 w, 1627 w, 2656 vs, 1520 vs, 1483 s, 1438 vs, 1368 vs, 1274 s, 1191 m, 1166 w, 1108 s, 1025 m, 996 m, 937 m, 789 w, 757 m, 723 s, 690 s, 645 m, 526 vs, 463 s, 432 w. UV–Vis (in CH<sub>2</sub>Cl<sub>2</sub>,  $\lambda_{\text{max}}$ ) 527, 396, 330, 295, 235 nm. HR-MS (ESI-TOF) found 577.7369 *m/z* (calcd for [M]<sup>+</sup> 577.6223). <sup>1</sup>H NMR (chloroform-*d*<sub>1</sub>, 298 K)  $\delta$  8.08 (m, 4H, *p*-H), 7.97 (m, 8H), 7.88 (m, 8H), 5.93 (s, 2H, CH), 2.50 (s, 6H, CH<sub>3</sub>) and 2.39 (s, 6H, CH<sub>3</sub>).

### 3.2.3. Synthesis of trans-Ph<sub>4</sub>P[Ru<sup>III</sup>(acac)<sub>2</sub>(NCS)<sub>2</sub>] (3·0.5C<sub>6</sub>H<sub>14</sub>)

A methanolic solution of **1** (0.60 g, 0.84 mmol) and KSCN (0.85 g, 8.76 mmol) was refluxed for 24 h. Then, the solution was evaporated to dryness and the residue was dissolved in dichloromethane and filtered. The filtrate was evaporated to ca. 3 mL, followed by the addition of *n*-hexane to give a reddish-purple precipitate, which was collected through filtration and dried under vacuum at 100 °C for 3 h. The yield was 0.43 g (64% based on *trans*-Ph<sub>4</sub>P[Ru(acac)<sub>2</sub>Cl<sub>2</sub>] (**1**)). Anal found: C, 58.94; H, 4.56; N, 3.75. calcd for C<sub>39</sub>H<sub>41</sub>N<sub>2</sub>O<sub>4</sub>S<sub>2</sub>PRu: C, 58.70; H, 5.18; N, 3.51. IR data (KBr disk, cm<sup>-1</sup>) 3057 w, 2087 vs, 2054 s, 1522 vs, 1483 m, 1436 s, 1378 s, 1270 m, 1188 w, 1108 s, 1024 m, 996 m, 935 m, 791 w, 754 m, 723 s, 689 m, 658 w, 526 vs, 456 m. UV–Vis (in CH<sub>2</sub>Cl<sub>2</sub>,  $\lambda_{\text{max}}$ ) 552, 464, 351, 276, 270, 237. HR-MS (ESI-TOF) found 415.9426 *m/z* (calcd for [M]<sup>+</sup> 415.4562). <sup>1</sup>H NMR (chloroform-*d*<sub>1</sub>, 298 K)  $\delta$  8.50–7.80 (m, *o,m,p*-H), –16.89 and –17.36 (s, CH<sub>3</sub>), –53.67 and –55.53 (s, CH<sub>3</sub>).

### 3.3. Crystal Structure Determination

X-ray crystallographic data for **1**, **2**·H<sub>2</sub>O and **3**·CH<sub>3</sub>CN (Table 1) were collected for each single crystal at 293 K on a RIGAKU Saturn 724 CCD system equipped with a Mo rotating-anode X-ray generator with monochromate Mo K $\alpha$  radiation ( $\lambda = 0.71075 \text{ \AA}$ ) (installed at the Okayama University of Science). The structures were solved using direct methods (SHELXT and SIR-2011, respectively) and refined using the full-matrix least-squares technique ( $F^2$ ) with SHELXL-2014 as part of the SAINT Crystal Structure 4.2.5 (RIGAKU) software, respectively. Non-hydrogen atoms were refined with anisotropic displacement parameters, and all hydrogen atoms were refined with a riding model [55,56]. Selected bond distances and angles for **1**, **2**·H<sub>2</sub>O and **3**·CH<sub>3</sub>CN are given in Tables S1–S6. CCDC-2325719, 2327661 and 2325718 contained the supplementary crystallographic data for *trans*-Ph<sub>4</sub>P[Ru<sup>III</sup>(acac)<sub>2</sub>Cl<sub>2</sub>] (**1**), Ph<sub>4</sub>P[*{Ru<sup>III</sup>(acac)Cl}\_2(\mu\text{-}Cl)*<sub>3</sub>]·H<sub>2</sub>O (**2**·H<sub>2</sub>O) and *trans*-Ph<sub>4</sub>P[Ru<sup>III</sup>(acac)<sub>2</sub>(NCS)<sub>2</sub>] (**3**·CH<sub>3</sub>CN), respectively. These data can be obtained free of charge from the Cambridge Crystallographic Data Centre via [www.ccdc.cam.ac.uk/data\\_request/cif](http://www.ccdc.cam.ac.uk/data_request/cif) (accessed on 31 January 2024).

## 4. Conclusions

The mononuclear and dinuclear ruthenium(III) complexes *trans*-Ph<sub>4</sub>P[Ru<sup>III</sup>(acac)<sub>2</sub>Cl<sub>2</sub>] (**1**) and Ph<sub>4</sub>P[*{Ru<sup>III</sup>(acac)Cl}\_2(\mu\text{-}Cl)*<sub>3</sub>] (**2**) were synthesized through the reactions of RuCl<sub>3</sub>·nH<sub>2</sub>O with acetylacetone. The dinuclear complex **2** was isolated by passing oxygen gas during the reaction and repeated chromatographic purifications using Al<sub>2</sub>O<sub>3</sub> columns (eluents: chloroform/MeOH and acetonitrile/chloroform). The mononuclear complex *trans*-Ph<sub>4</sub>P[Ru<sup>III</sup>(acac)<sub>2</sub>(NCS)<sub>2</sub>]·0.5C<sub>6</sub>H<sub>14</sub> (**3**·0.5C<sub>6</sub>H<sub>14</sub>) was synthesized through the substitution reaction of the axial Cl<sup>−</sup> of **1** with NCS<sup>−</sup>. The mononuclear structures of **1** and **3**·CH<sub>3</sub>CN and a dinuclear structure of **2**·H<sub>2</sub>O were confirmed through X-ray crystal structure analyses. The Ru–Ru distance of 2.6661(2) in the dinuclear core of **2**·H<sub>2</sub>O was indicative of the existence of the direct metal–metal interaction. The room temperature magnetic moments ( $\mu_{\text{eff}}$ ) were 2.00 and 1.93  $\mu_{\text{B}}$  for **1** and **3**·0.5C<sub>6</sub>H<sub>14</sub>, respectively, and 0.66  $\mu_{\text{B}}$  for **2**. The strong antiferromagnetic interaction ( $J \leq -800 \text{ cm}^{-1}$ ) between the ruthenium(III) ions within the dinuclear core was confirmed with a temperature-dependent magnetic susceptibility measurement at the 2–300 K range. The field dependence for magnetization measured from 0 to 70,000 Oe at 2 K showed that **2** was typical of the one for diamagnetism due to the strong antiferromagnetic interaction. The strong antiferromagnetic interaction between the unpaired electrons of the ruthenium(III) centers was considered to come from the direct metal–metal interaction. The mononuclear and dinuclear cores of **1**, **2**, and **3**·C<sub>6</sub>H<sub>14</sub> were maintained in the solution of CH<sub>2</sub>Cl<sub>2</sub>, which was verified by similarity in the absorption band positions in the visible region between the spectra measured in solid (diffuse reflectance spectrum) and solution (absorption spectrum) for each complex. In the <sup>1</sup>H NMR spectra measured in chlroform-*d*<sub>1</sub> at 298 K, the dinuclear complex **2** showed signals for the acac ligand protons at 5.93 ppm (for CH) and 2.50 and 2.39 ppm (for CH<sub>3</sub>), respectively, while **1** and **3**·0.5C<sub>6</sub>H<sub>14</sub> showed signals with large paramagnetic shifts: −17.59 ppm (for CH<sub>3</sub>) and −57.01 ppm (for CH) for **1** and −16.89 and −17.36 ppm (for CH<sub>3</sub>) and −53.67 and −55.53 ppm (for CH) for **3**·0.5C<sub>6</sub>H<sub>14</sub>. In the CVs (the potential was quoted relative to the Fc/Fc<sup>+</sup> couple), which were measured in CH<sub>2</sub>Cl<sub>2</sub> with an electrolyte of <sup>n</sup>Bu<sub>4</sub>N(ClO<sub>4</sub>), the Ru<sup>III</sup> → Ru<sup>IV</sup> redox wave was shown at 0.23 V for **1**, but not for **3**·0.5C<sub>6</sub>H<sub>14</sub> due to the decomposition, and Ru<sup>III</sup> → Ru<sup>II</sup> waves were shown at −1.39 V for **1** and −1.25 V for **3**·0.5C<sub>6</sub>H<sub>14</sub>, while, for **2**, the Ru<sup>III</sup>–Ru<sup>III</sup> → Ru<sup>III</sup>–Ru<sup>IV</sup> and Ru<sup>III</sup>–Ru<sup>III</sup> → Ru<sup>III</sup>–Ru<sup>IV</sup> waves were shown at 0.91 V and −0.79 V, respectively.

**Supplementary Materials:** The following supporting information can be downloaded at: <https://www.mdpi.com/article/10.3390/magnetochemistry10030016/s1>, Table S1: Bond lengths of **1**; Table S2: Bond angles of **1**; Table S3: Bond lengths of **2**·H<sub>2</sub>O; Table S4: Bond angles of **2**·H<sub>2</sub>O; Table S5: Bond lengths of **3**·CH<sub>3</sub>CN; Table S6: Bond angles of **3**·CH<sub>3</sub>CN; Figure S1: IR spectrum of **1**; Figure S2: IR spectrum of **2**; Figure S3: IR spectrum of **3**·0.5C<sub>6</sub>H<sub>14</sub>; Figure S4: Observed (top) and simulated (bottom) XRD

patterns of **1**; Figure S5: Observed (top for **2**) and simulated (bottom for  $2 \cdot \text{H}_2\text{O}$ ) XRD patterns; Figure S6: Observed (top for  $3 \cdot 0.5\text{C}_6\text{H}_{14}$ ) and simulated (bottom for  $3 \cdot \text{CH}_3\text{CN}$ ) XRD patterns; Figure S7: Crystal packing diagram of **1** without hydrogen for clarity; Figure S8: Packing diagram of  $2 \cdot \text{H}_2\text{O}$  without hydrogen atoms for clarity; Figure S9: Packing diagram of  $3 \cdot \text{CH}_3\text{CN}$  without hydrogen atoms for clarity; Figure S10: Field dependence of magnetization for **1** at 2 K. The red solid line represents the Brillouin function with  $g = 2.3$ ; Figure S11: Field dependence of magnetization for **2** at 2 K; Figure S12: Field dependence of magnetization for  $3 \cdot 0.5\text{C}_6\text{H}_{14}$  at 2 K. The red solid line represents the Brillouin function with  $g = 2.1$ ; Figure S13: Diffuse reflectance spectra of **1** (orange solid line), **2** (blue solid line) and  $3 \cdot 0.5\text{C}_6\text{H}_{14}$  (green solid line); Figure S14:  $^1\text{H}$  NMR Spectrum of **1** in chloform- $d_1$  at 298 K; Figure S15:  $^1\text{H}$  NMR spectrum of **2** in chloform- $d_1$  at 298 K; Figure S16:  $^1\text{H}$  NMR spectrum of  $3 \cdot 0.5\text{C}_6\text{H}_{14}$  in chloform- $d_1$  at 298 K.

**Author Contributions:** Conceptualization, methodology and funding acquisition, M.H.; investigation, K.N., C.H., S.N., H.A. and M.M.; data curation, M.H.; writing—original draft preparation, K.N. and M.H.; writing—review and editing, M.H. All authors have read and agreed to the published version of the manuscript.

**Funding:** A part of this work (SQUID measurement) was conducted at the Institute for Molecular Science, supported by Advanced Research Infrastructure for Materials and Nanotechnology in Japan (JPMXP1223MS1053) of the Ministry of Education, Culture, Sport, Science and Technology (MEXT), Japan.

**Institutional Review Board Statement:** Not applicable.

**Informed Consent Statement:** Not applicable.

**Data Availability Statement:** Crystallographic data of **1**,  $2 \cdot \text{H}_2\text{O}$  and  $3 \cdot \text{CH}_3\text{CN}$  can be obtained free of charge from the Cambridge Crystallographic Data Centre (CCDC); deposition numbers of **1**, **2** and  $3 \cdot \text{CH}_3\text{CN}$  are CCDC-2325719, 2327661 and 2325718, respectively.

**Acknowledgments:** The authors are grateful to Michiko Egawa (Shimane University) for her measurements of the elemental analyses, Masataka Maeyama (Rigaku Corporation) for his useful suggestion in the crystal structure analysis of complex  $2 \cdot \text{H}_2\text{O}$  and Yusuke Kataoka (Shimane University) for his help to measure the field-dependent magnetization and PXRD.

**Conflicts of Interest:** The authors declare no conflicts of interest.

## References

- Chen, G.J.-J.; McDonald, J.W.; Newton, W.E. Preparation of  $\text{OMoCl}(\text{acac})_2$  by a novel oxygen-chlorine atom exchange and its use as a reagent for the synthesis of monomeric molybdenum(V) complexes. *Inorg. Chim. Acta* **1979**, *35*, 93–97. [[CrossRef](#)]
- Doyle, G. The Reaction of Some Molybdenum and Tungsten Halides with  $\beta$ -Diketones. *Inorg. Chem.* **1971**, *10*, 2348–2350. [[CrossRef](#)]
- Dallmann, K.; Preetz, W. Crystal Structures, Vibrational Spectra and Normal Coordinate Analyses of *cis*- and *trans*-[ $\text{OsX}_2(\text{acac})_2$ ], X = Cl, Br, I. *Z. Für Naturforschung B* **1997**, *52*, 965–974. [[CrossRef](#)]
- Young, K.J.H.; Mironov, O.A.; Nielsen, R.J.; Chen, M.J.; Stewart, T.; Goddard, W.A., III; Periana, R.A. Synthesis and Characterization of the  $\kappa^2$ -acac-O,O Complex  $\text{Os}^{IV}(\text{acac})_2\text{PhCl}$  and Study of CH Activation with Benzene. *Organometallics* **2011**, *30*, 5088–5094. [[CrossRef](#)]
- Ferguson, G.; Glidewell, C. Enantiomeric disorder in racemic *cis* dichlorobis(pentane-2,4-dionato) titanium(IV). *Acta Cryst.* **2001**, *C57*, 264–265.
- Wilkie, C.A.; Lin, G.Y.; Haworth, D.T. A comparative study of the *cis*-disubstituted bis( $\beta$ -diketonato)titanium(IV) complexes. *J. Inorg. Nucl. Chem.* **1978**, *40*, 1009–1012. [[CrossRef](#)]
- Lindmark, A.F.; Fay, R.C. Dipseudohalobis ( $\beta$ -diketonato)titanium(IV) complexes. Synthesis, stereochemistry, configurational rearrangements, and vibrational spectra. *Inorg. Chem.* **1975**, *14*, 282–287. [[CrossRef](#)]
- Bradley, D.C.; Holloway, C.E. Nuclear magnetic resonance and infrared spectral studies on labile *cis*-dialkoxy-bis(acetylacetone) titanium(IV) compounds. *J. Chem. Soc. A* **1969**, 282–285. [[CrossRef](#)]
- Brown, S.N.; Chu, E.T.; Hull, M.W.; Noll, B.C. Electronic Dissymmetry in Chiral Recognition. *J. Am. Chem. Soc.* **2005**, *127*, 16010–16011. [[CrossRef](#)] [[PubMed](#)]
- Fay, R.C.; Lowry, R.N. Structure and lability of dihalobis(acetylacetone)titanium(IV) complexes. *Inorg. Nucl. Chem. Lett.* **1967**, *3*, 117–120. [[CrossRef](#)]
- Cox, M.; Clark, R.J.H.; Milledge, H.J. Structural Studies on Group IV Metal Acetylacetones. *Nature* **1966**, *212*, 1357. [[CrossRef](#)]
- Sarkhel, P.; Paul, B.C.; Poddar, R.K. Rhodium(III) complexes containing acetylacetone and mono- or bidentate ligands. *Indian J. Chem.* **1999**, *38A*, 150–155.

13. Sodhi, R.K.; Paul, S. An Overview of Metal Acetylacetones: Developing Areas/Routes to New Materials and Applications in Organic Syntheses. *Catal. Surv. Asia* **2018**, *22*, 31–62. [[CrossRef](#)]
14. Behzadi, K.; Thompson, A. Preparation, Characterization and Reactions of Vanadium(IV)  $\beta$ -Diketonate Complexes. *J. Less Common Met.* **1987**, *128*, 281–296. [[CrossRef](#)]
15. Paul, B.C.; Poddar, R.K. Synthesis, characterization and reactivity studies of dichloroacetylacetone acetylacetone ruthenium(III). *Transit. Met. Chem.* **1993**, *18*, 96–100. [[CrossRef](#)]
16. Janiak, C.; Scharmann, T.G.; Lange, C.H.K. Zirconium  $\beta$ -diketonate/methylaluminoxane systems as singlesite catalysts for the preparation of high-molecular-weight polyethylene. *Macromol. Rapid Commun.* **1994**, *15*, 655–658. [[CrossRef](#)]
17. Pinnavia, T.J.; Fay, R.C. Preparation and properties of some six- and seven-coordinate halo(acetylacetato) complexes of zirconium(IV) and hafnium(IV). *Inorg. Chem.* **1968**, *7*, 502–508. [[CrossRef](#)]
18. Bagnall, K.W.; Edwards, J.; Rickard, C.E.F.; Tempest, A.C. Cyclopentadienyluranium(IV) acetylacetonates. *J. Inorg. Nucl. Chem.* **1979**, *41*, 1321–1323. [[CrossRef](#)]
19. Shibata, S.; Ohta, M. Molecular structure of bis(acetylacetato)zinc(II) in the gas phase as determined from electron diffraction data. *J. Mol. Struct.* **1981**, *77*, 265–270. [[CrossRef](#)]
20. Korochentsev, V.V.; Vovna, V.I.; L'vov, I.B.; Shapkin, N.P. Electronic and geometric structure of the protonated forms of nickel  $\beta$ -diketonates. *Russ. J. Coord. Chem.* **2011**, *37*, 371–376. [[CrossRef](#)]
21. Funaioli, T.; Marchetti, F.; Pampaloni, G.; Zacchini, S. Ligand-interchange reactions between M(iv) ( $M = Ti, V$ ) oxide bis-acetylacetonates and halides of high-valent group 4 and 5 metals. A synthetic and electrochemical study. *Dalton Trans.* **2013**, *42*, 14168–14177. [[CrossRef](#)]
22. Stabinikov, P.A.; Pervukhina, N.V.; Baidina, I.A.; Sheludyakova, L.A.; Borisov, S.V. On the Symmetry of iron(III) tris-acetylacetone crystals. *J. Struct. Chem.* **2007**, *48*, 186–192. [[CrossRef](#)]
23. Shalhoub, G.M. Co(acac)<sub>3</sub> Synthesis, reactions, and spectra: An experiment for general chemistry. *J. Chem. Educ.* **1980**, *57*, 525–526. [[CrossRef](#)]
24. Ledneva, A.Y.; Artemkina, S.B.; Piryazev, D.A.; Fedorov, V.E. Structure and Thermal Properties of the molybdenum Complex Mo(acac)<sub>3</sub>. *J. Struct. Chem.* **2015**, *56*, 1021–1023. [[CrossRef](#)]
25. Dedeian, K.; Djurovich, P.I.; Garces, F.O.; Carlson, G.; Watts, R.J. A new synthetic route to the preparation of a series of strong photoreducing agents: Fac-tris-ortho-metallated complexes of iridium(III) with substituted 2-phenylpyridines. *Inorg. Chem.* **1991**, *30*, 1685–1687. [[CrossRef](#)]
26. Dallmann, K.; Preetz, W. Darstellung, Kristallstruktur, Schwingungsspektren und Normalkoordinatenanalyse von [Os(acac)<sub>3</sub>]/Synthesis, Crystal Structure, Vibrational Spectra, and Normal Coordinate Analysis of [Os(acac)<sub>3</sub>]. *Z. Für Naturforschung B* **1998**, *53*, 232–238. [[CrossRef](#)]
27. Jackson, A.B.; White, P.S.; Templeton, J.L. Bis(acetylacetato)tricarbonyl Tungsten(II): A Convenient Precursor to Chiral Bis(acac) Tungsten(II) Complexes. *Inorg. Chem.* **2006**, *45*, 6205–6213. [[CrossRef](#)] [[PubMed](#)]
28. Chang, Q.; Yan, C.; Li, X.-N.; Cui, H.; Ye, Q.; Jiang, J.; Yu, J.; Chen, J.; Liu, W. The influence of sodium and barium ions on the structures of iridium (III) acetylacetone complexes. *Res. Chem. Intermed.* **2015**, *41*, 7631–7640. [[CrossRef](#)]
29. Nakanishi, R.; Yatoo, M.A.; Katoh, K.; Breedlove, B.K.; Yamashita, M. Dysprosium Acetylacetato Single-Molecule Magnet Encapsulated in Carbon Nanotubes. *Materials* **2017**, *10*, 7. [[CrossRef](#)]
30. Zhang, D.; Zhang, L.-F.; Yuting, C.; Hailong, W.; Ni, Z.-H.; Wolfgang, W.; Jianzhuang, J. Heterobimetallic porphyrin-based single-chain magnet constructed from manganese(iii)-porphyrin and trans-dicyanobis(acetylacetato) ruthenate(iii) containing co-crystallized bulk anions and cations. *Chem. Commun.* **2010**, *46*, 3550–3552. [[CrossRef](#)]
31. Lan, W.; Hao, X.; Dou, Y.; Zhou, Z.; Yang, L.; Liu, H.; Li, D.; Dong, Y.; Kong, L.; Zhang, D. Various Structural Types of Cyanide-Bridged Fe<sup>III</sup>–Mn<sup>III</sup> Bimetallic Coordination Polymers (CPs) and Polynuclear Clusters Based-on A New mer-Tricyanoiron(III)Building Block: Synthesis, Crystal Structures, and Magnetic Properties. *Polymers* **2019**, *11*, 1585. [[CrossRef](#)]
32. Hirayama, M.; Kitani, K. Observation of <sup>27</sup>Al n.m.r. paramagnetic shifts (large contact shift contributions) induced by lanthanoid shift-reagents in tris(acetylacetato)aluminium(III). *J. Chem. Soc. Chem. Commun.* **1980**, *21*, 1030–1031. [[CrossRef](#)]
33. Goff, H.M.; Hines, J.; Griesel, J.; Mossman, C. Synthesis, Characterization, and Use of a Cobalt(II) Complex as an NMR Shift Reagent. *J. Chem. Educ.* **1982**, *59*, 422–423. [[CrossRef](#)]
34. Levy, G.C.; Komoroski, R.A. Paramagnetic Relaxation Reagents. Alternatives or Complements to Lanthanide Shift Reagents in Nuclear Magnetic Resonance Spectral Analysis. *J. Am. Chem. Soc.* **1974**, *96*, 678–681. [[CrossRef](#)]
35. Gillies, E.; Szarek, W.A.; Baird, M.C. Application of Paramagnetic Shift Reagents in Nuclear Magnetic Resonance Studies of Complex Alcohols and Amines. *Can. J. Chem.* **1971**, *49*, 211–216. [[CrossRef](#)]
36. Sirkecioglu, O.; Karlige, B.; Talinli, N. Benzylation of alcohols by using bis[acetylacetato]copper as catalyst. *Tetrahedron Lett.* **2003**, *44*, 8483–8485. [[CrossRef](#)]
37. Pichugina, D.; Kuz'menko, N.; Shestakov, A. Gold complexes with Oxygen-containing Ligands as a Catalyst for Methane Oxidation. *Gold Bull.* **2007**, *40*, 115–120. [[CrossRef](#)]
38. Yeung, W.-F.; Man, W.-L.; Wong, W.-T.; Lau, T.-C.; Gao, S. Ferromagnetic Ordering in a Diamond-Like Cyano-Bridged Mn<sup>II</sup>Ru<sup>III</sup> Bimetallic Coordination Polymer. *Angew. Chem. Int. Ed.* **2001**, *40*, 3031–3033. [[CrossRef](#)]

39. Guo, J.-F.; Wang, X.-T.; Wang, B.-W.; Xu, G.-C.; Gao, S.; Szeto, L.; Wong, W.-T.; Wong, W.-Y.; Lau, T.-C. One-Dimensional Ferromagnetically Coupled Bimetallic Chains Constructed with *trans*-[Ru(acac)<sub>2</sub>(CN)<sub>2</sub>]<sup>−</sup>: Syntheses, Structures, Magnetic Properties, and Density Functional Theoretical Study. *Chem. Eur. J.* **2010**, *16*, 3524–3535. [[CrossRef](#)]
40. Hasegawa, T.; Lau, T.C.; Taube, H.; Schaefer, W.P. Electronic Effects of Bis(acetylacetone) in Ruthenium(II) and Ruthenium(III) Complexes. *Inorg. Chem.* **1991**, *30*, 2921–2928. [[CrossRef](#)]
41. Darriet, J. Crystal structure and magnetic properties of the (Ru<sub>2</sub>Cl<sub>9</sub>)<sup>3−</sup> ion in Cs<sub>3</sub>Ru<sub>2</sub>Cl<sub>9</sub>. *Rev. Chim. Mine.* **1981**, *18*, 27–32.
42. Hughes, M.N.; O'Reardon, D.; Poole, R.K.; Hursthouse, M.B.; Thornton-Pett, M. The Structure of the mixed-valence chloro-bridged dimeric complex cation [Ru<sub>2</sub>(NH<sub>3</sub>)<sub>6</sub>Cl<sub>3</sub>]<sup>2+</sup>. *Polyhedron* **1987**, *6*, 1711–1713. [[CrossRef](#)]
43. Clucas, W.A.; Armstrong, R.S.; Buys, I.E.; Hambley, T.W.; Nugent, K.W. X-ray Crystallographic Study of the Ruthenium Blue Complexes [Ru<sub>2</sub>Cl<sub>3</sub>(tacn)<sub>2</sub>](PF<sub>6</sub>)<sub>2</sub>·H<sub>2</sub>O, [Ru<sub>2</sub>Br<sub>3</sub>(tacn)<sub>2</sub>](PF<sub>6</sub>)<sub>2</sub>·H<sub>2</sub>O, and [Ru<sub>2</sub>I<sub>3</sub>(tacn)<sub>2</sub>](PF<sub>6</sub>)<sub>2</sub>: Steric Interactions and the Ru-Ru “Bond Length”. *Inorg. Chem.* **1996**, *35*, 6789–6794. [[CrossRef](#)] [[PubMed](#)]
44. Neubold, P.; Vedova, B.S.P.C.D.; Wieghardt, K.; Nuber, B.; Weiss, J. Novel Cofacial Bioctahedral Complexes of Ruthenium: Syntheses and Properties of the Mixed-Valence Species [LRu<sup>2.5</sup>(μ-X)<sub>3</sub>Ru<sup>2.5</sup>L]<sup>2+</sup> (X = Cl, Br, I, OH). Crystal Structures of [LRu<sup>2.5</sup>(μ-OH)<sub>3</sub>Ru<sup>2.5</sup>L](PF<sub>6</sub>)<sub>2</sub>·H<sub>2</sub>O and [LRu<sup>IV</sup>(μ-O)<sub>3</sub>Ru<sup>IV</sup>L](PF<sub>6</sub>)<sub>2</sub>·H<sub>2</sub>O (L = 1,4,7-Trimethyl-1,4,7-triazacyclononane). *Inorg. Chem.* **1990**, *29*, 3355–3363.
45. Bonner, J.C.; Fisher, M.E. Linear Magnetic Chains with Anisotropic Coupling. *Phys. Rev.* **1964**, *135*, 640–658. [[CrossRef](#)]
46. Bleaney, B.; Bowers, K.D. Anomalous paramagnetism of copper acetate. *Proc. R. Soc. Lond.* **1952**, *214*, 451–465. [[CrossRef](#)]
47. Lovel, T.; Stranger, R.; McGrady, J.E. Mutual Interdependence of Spin Crossover and Metal-Metal Bond Formation in M<sub>2</sub>Cl<sub>9</sub><sup>3−</sup> (M = Fe, Ru, Os). *Inorg. Chem.* **2001**, *40*, 39–43. [[CrossRef](#)]
48. Cotton, F.A.; Matusz, M.; Torralba, R.C. New Di- and Trinuclear Complexes of Ruthenium with Octahedra Joined on Faces or Edges: Ru<sub>2</sub>Cl<sub>6</sub>(PBu<sub>3</sub>)<sub>3</sub>, Ru<sub>2</sub>Cl<sub>6</sub>(PBu<sub>3</sub>)<sub>4</sub> and Ru<sub>3</sub>Cl<sub>8</sub>(PBu<sub>3</sub>)<sub>4</sub> (Bu = CH<sub>3</sub>CH<sub>2</sub>CH<sub>2</sub>CH<sub>2</sub>). *Inorg. Chem.* **1989**, *28*, 1516–1520. [[CrossRef](#)]
49. Grobelny, R.; Jezowska-Trzebiatowska, B.; Wojciechowski, W. The Absorption Spectra and Magnetic Properties of the chelated compounds of Ru(III) with β-diketones. *J. Inorg. Nucl. Chem.* **1966**, *28*, 2715–2718. [[CrossRef](#)]
50. Cardona, C.M.; Li, W. Electrochemical Considerations for Determining Absolute Frontier Orbital Energy Levels of Conjugated Polymers for Solar Cell Applications. *Adv. Mater.* **2011**, *23*, 2367–2371. [[CrossRef](#)]
51. Hashem, E.; Platts, J.A.; Hartl, F.; Lorusso, G.; Evangelisti, M.; Schulzke, C.; Baker, R.J. Thiocyanate Complexes of Uranium in Multiple Oxidation States: A Combined Structural, Magnetic, Spectroscopic, Spectroelectrochemical, and Theoretical Study. *Inorg. Chem.* **2014**, *53*, 8624–8637. [[CrossRef](#)]
52. Bain, G.A.; Berry, J.F. Diamagnetic Corrections and Pascal's Constants. *J. Chem. Educ.* **2008**, *85*, 532–536. [[CrossRef](#)]
53. Gottlieb, H.E.; Kotlyar, V.; Nudelman, A. NMR Chemical Shifts of Common Laboratory Solvents as Trace Impurities. *J. Org. Chem.* **1997**, *62*, 7512–7515. [[CrossRef](#)]
54. Fulmer, G.R.; Miller, A.J.M.; Sherden, N.H.; Hugo, E.G.; Nudelman, A.; Brian, M.S.; John, E.B.; Karen, I.G. NMR Chemical Shifts of Trace Impurities: Common Laboratory Solvents, Organics, and Gases in Deuterated Solvents Relevant to the Organometallic Chemist. *Organometallics* **2010**, *29*, 2176–2179. [[CrossRef](#)]
55. Sheldrick, G.M. SHELXT—Integrated space-group and crystal-structure determination. *Acta Cryst.* **2015**, *A71*, 3–8. [[CrossRef](#)] [[PubMed](#)]
56. Sheldrick, G.M. Crystal structure refinement with SHELXL. *Acta Cryst.* **2015**, *C71*, 3–8.

**Disclaimer/Publisher's Note:** The statements, opinions and data contained in all publications are solely those of the individual author(s) and contributor(s) and not of MDPI and/or the editor(s). MDPI and/or the editor(s) disclaim responsibility for any injury to people or property resulting from any ideas, methods, instructions or products referred to in the content.